ISSN (Print) 1226-1750
ISSN (Online) 2233-6656
Journal of Magnetics 30(4), 794-801 (2025) https://doi.org/10.4283/JMAG.2025.30.4.794

TransMorph-Inspired Hybrid CNN–MLP 3D Rigid Registration for Adaptive Radiotherapy

Byungdu Jo*

Department of Radiological Science, Dongseo University, Busan 47011, Republic of Korea
Center for Radiological Environment & Health Science, Dongseo University, Busan 47011, Republic of Korea

(Received 6 November 2025, Received in final form 4 December 2025, Accepted 4 December 2025)

Accurate alignment between cone-beam computed tomography (CBCT) and simulation computed tomography (Sim-CT) is essential for precise dose delivery in adaptive radiotherapy (ART). However, conventional intensity-based registration remains limited by CBCT-specific degradations such as scatter, beam hardening, and nonlinear intensity distortions. This study proposes a 3D deep-learning–based rigid registration framework optimized for robust CBCT-to-Sim-CT alignment. A paired dataset was generated using the Tomographic Iterative GPU-based Reconstruction Toolbox (TIGRE) with controlled fan-beam and cone-beam geometries under six-degree-of-freedom (6-DoF) motion. The hybrid Convolutional Neural Network–Multi-Layer Perceptron (CNN–MLP) model directly estimated rigid transformation parameters through end-to-end learning with a composite loss combining Structural Similarity Index Measure (SSIM), Normalized Cross-Correlation (NCC), Mutual Information (MI), and gradient regularization. The framework achieved sub-millimeter and sub-degree accuracy with stable convergence and robustness against CBCT-specific nonlinearities. These findings demonstrate the potential of this physics-informed, GPU-accelerated approach for accurate and efficient alignment in real-time adaptive radiotherapy workflows.

Keywords : cone-beam computed tomography, rigid registration, adaptive radiotherapy, electromagnetic radiation, structural similarity

1. Introduction

In external-beam radiotherapy (EBRT), accurate patient positioning and anatomical alignment are essential to ensure that the prescribed dose conforms precisely to the target while minimizing exposure to surrounding organs at risk (OARs) [1]. Even small setup errors or anatomical changes between fractions can cause significant deviations in dose distribution, reducing tumor control probability and increasing normal tissue complication risks [2]. To mitigate these uncertainties, image-guided radiotherapy (IGRT) is routinely employed, with on-board cone-beam computed tomography (CBCT) serving as the primary imaging modality for daily patient verification [3]. CBCT provides volumetric imaging for setup correction in six degrees of freedom and enables adaptive workflows. However, compared with fan-beam simulation computed tomography (Sim-CT), CBCT suffers from scatter, beam hardening, truncated field-of-view, and low soft-tissue contrast [4, 5]. These physical limitations degrade image quality and compromise the robustness of intensity-based registration between CBCT and Sim-CT, particularly in soft-tissue–dominant regions such as the head and neck or pelvis [6]. In adaptive radiotherapy (ART) workflows, image registration provides the spatial correspondence between daily images and the planning CT, which is required for dose accumulation, contour propagation, and subsequent plan adaptation [7]. Conventional registration algorithms, including mutual information and cross-correlation, rely heavily on intensity similarity [8]. As a result, they often fail under CBCT-specific conditions such as noise, scatter-induced non-linear intensity distortions, and anatomical truncation [3, 4, 9, 10]. Moreover, their iterative optimization process can be computationally expensive and impractical for time-sensitive adaptive workflows [11]. Deep learning–based registration has recently emerged as a powerful alternative by learning image features that capture structural and contextual

*Corresponding author: Tel: +82-51-320-4274
e-mail: byungdujo@gdsu.dongseo.ac.kr

correspondence beyond raw intensity [12]. Methods such as VoxelMorph and TransMorph have achieved high accuracy and speed in deformable registration tasks [13, 14]. While these approaches focus on modeling non-rigid anatomical variations, rigid registration remains the essential first step in clinical radiotherapy workflows, providing a geometrically consistent reference that precedes any deformable registration or dose recalculation [8, 13, 14]. Traditional rigid registration methods, however, still depend on hand-crafted similarity metrics and struggle when image intensity distributions differ substantially between modalities, as in CBCT and Sim-CT [5, 6]. In this study, we propose a deep-learning-based rigid registration framework specifically designed for CBCT-to-Sim-CT alignment in adaptive radiotherapy. The objective of this framework is to achieve robust geometric correspondence between fan-beam Sim-CT and CBCT volumes reconstructed at different spatial resolutions and contrast conditions. To enable quantitative and reproducible evaluation, a paired dataset with known transformations was generated using the Tomographic Iterative GPU-based Reconstruction Toolbox (TIGRE) under controlled imaging geometry [15]. Building upon the TransMorph paradigm, a lightweight hybrid Convolutional Neural Network–Multi-Layer Perceptron (CNN–MLP) architecture was developed to directly estimate six rigid transformation parameters, ensuring physically interpretable and computationally efficient alignment without voxel-wise deformation. The model was trained with a composite loss function integrating Structural Similarity (SSIM), Normalized Cross-Correlation (NCC), Mutual Information (MI), and gradient regularization to enhance structural fidelity and stability across heterogeneous imaging conditions.

This framework aims to provide a reproducible and physics-informed foundation for geometry-consistent, data-driven rigid alignment between CBCT and Sim-CT, supporting subsequent deformable registration and dose adaptation in modern adaptive radiotherapy workflows.

2. Materials and Methods

2.1. Dataset and Preprocessing

In this study, a dedicated dataset was generated using the TIGRE (Tomographic Iterative GPU-based Reconstruction Toolbox) under a fully controlled imaging environment. A modified Shepp–Logan phantom was implemented in Python and forward-projected using both fan-beam and cone-beam geometries. The overall data-generation geometry is illustrated in Fig. 1, while the six-degree-of-freedom (6-DoF) rigid-body motions applied to the phantom are shown in Fig. 2. The simulation CT (Sim-CT) volumes, serving as ground-truth references, were reconstructed with the fan-beam–based filtered back-projection (FBP) algorithm on a 256 × 256 × 256 grid with 1.0 mm^3 isotropic voxels. To ensure consistency, both FBP and Feldkamp–Davis–Kress (FDK) reconstructions were performed using identical geometry (SOD = 800 mm, SDD = 1200 mm), maintaining uniform magnification and spatial correspondence. The on-board imager (OBI)–based CBCT datasets, representative of clinical radiotherapy systems, were reconstructed using the FDK algorithm on a 128 × 128 × 128 grid with the same voxel size. To simulate patient setup uncertainties in adaptive radiotherapy, the phantom underwent controlled 3D translational (±1.5 cm, 0.5 cm steps) and rotational ($\leq 30^{o}$) transformations, including single- and multi-axis perturbations. Each transformed phantom was forward-projected and reconstructed with both FDK (CBCT) and FBP (Sim-CT) within the TIGRE framework. The resulting paired CBCT and Sim-CT volumes formed a standardized dataset for quantitative evaluation of the proposed 3D rigid registration network.

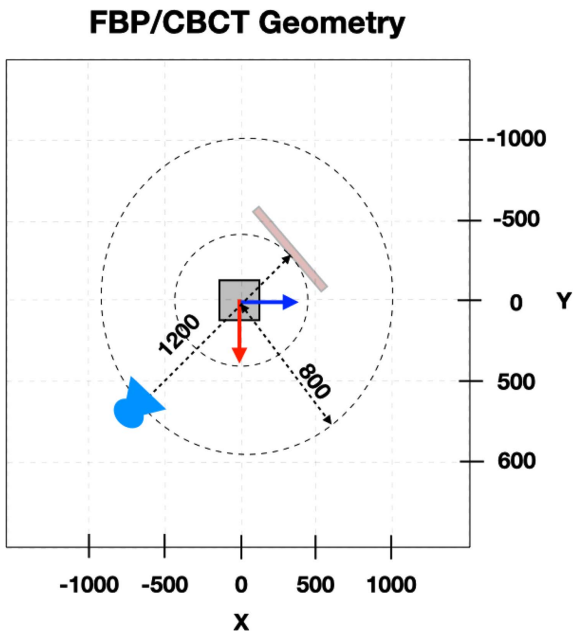

Fig. 1. (Color online) Schematic illustration of the imaging geometry used for data generation. A modified Shepp–Logan phantom was placed at isocenter and forward-projected under identical cone-beam CT (CBCT) and simulation CT (FBP) configurations. Source–object distance (SOD) and source-to-detector distance (SDD) were fixed at 800 mm and 1200 mm, respectively. Controlled translational and rotational offsets were applied to simulate patient-setup variations in adaptive radiotherapy.

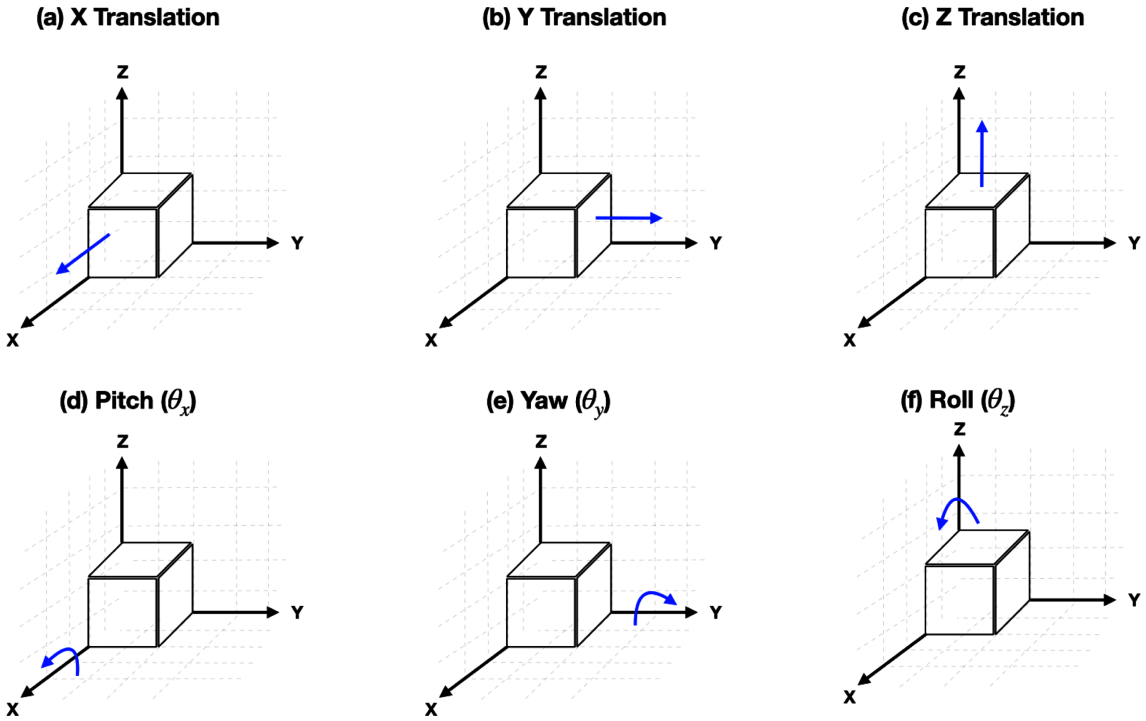

Fig. 2. (Color online) Overview of the six-degree-of-freedom (6-DoF) rigid-body transformations applied to the phantom during dataset generation. Panels (a)–(c) represent translational motions along the X, Y, and Z axes, while (d)–(f) illustrate rotational motions (pitch θ_x, yaw θ_y, and roll θ_z) about the corresponding axes.

2.2. Network Architecture

The overall structure of the proposed 3D rigid registration network is shown in Fig. 3. Inspired by the TransMorph framework for learning-based medical image registration [14], the model adopts a hybrid CNN–MLP design that directly predicts six rigid transformation parameters between CBCT and simulation CT (Sim-CT) volumes. Each input pair—moving (I_{mov}) and fixed (I_{fix})—is processed through a shared-weight 3D CNN dual encoder that extracts spatial features from both domains

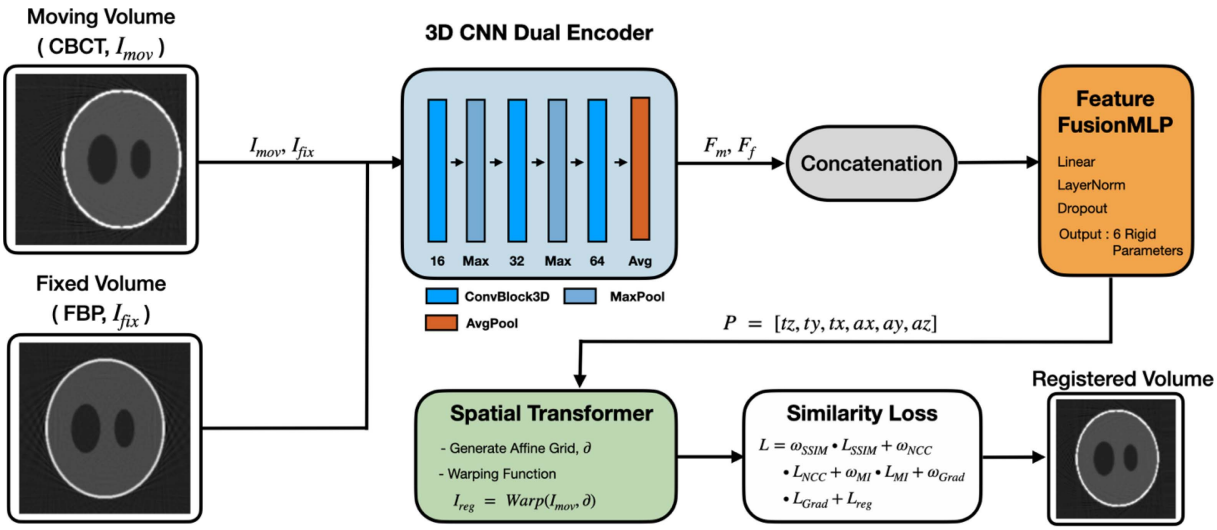

Fig. 3. (Color online) Overall architecture of the proposed TransMorph-inspired 3D rigid registration network. The model integrates dual-encoder convolutional feature extraction and a compact multilayer perceptron (MLP)-based fusion module to directly estimate six rigid transformation parameters between the moving (CBCT) and fixed (Sim-CT) volumes.

while maintaining consistent receptive-field characteristics. The encoded feature vectors (F_m, F_f) are concatenated and fused through a compact feature fusion MLP, which captures inter-volume correlations in a shared latent space with reduced computational cost. The MLP outputs six rigid parameters [Δx, Δy, Δz, θx, θy, θz] representing translation and rotation. Rotational terms are constrained by a scaled tanh activation to maintain realistic motion ranges. The predicted parameters are then converted into an affine transformation matrix within a Spatial Transformer Network (STN), which generates a sampling grid and performs differentiable warping of I_{mov} to produce the registered volume (I_{reg}). A composite similarity loss—comprising SSIM, NCC, MI, gradient, and regularization terms (Section 2.3)—quantifies the alignment between I_{reg} and I_{fix}. Because all operations are differentiable, the loss gradients are back-propagated through the STN, MLP, and CNN encoders, enabling end-to-end optimization of the 6-DoF rigid registration.

2.3. Loss Function

The proposed model was trained using a multi-term composite loss function designed to jointly enforce structural preservation, intensity alignment, and modality-invariant consistency between CBCT and Sim-CT volumes. Each loss term captures a distinct property of the registration process, ensuring stable convergence even under the non-linear intensity distributions and noise characteristics typical of CBCT images. The total objective function is expressed as:

$$\mathcal{L} = \omega_{SSIM} \cdot \mathcal{L}_{SSIM} + \omega_{NCC} \cdot \mathcal{L}_{NCC} + \omega_{MI} \cdot \mathcal{L}_{MI} + \omega_{Grad} \cdot \mathcal{L}_{Grad} + \mathcal{L}_{reg} \quad (1)$$

Here, $\mathcal{L}_{SSIM}$ represents the SSIM–based loss, which emphasizes preservation of anatomical structure and local contrast relationships. SSIM measures pixel-wise luminance, contrast, and structural correlation within local neighborhoods [16]. It is defined as:

$$SSIM(I_1, I_2) = \frac{(2\mu_1\mu_2 + C_1)(2\sigma_{12} + C_2)}{(\mu_1^2 + \mu_2^2 + C_1)(\sigma_1^2 + \sigma_2^2 + C_2)} \quad (2)$$

where μ_1, μ_2 and σ_2, σ_2 denote the local means and variances of I_1 and I_2, respectively, and σ_{12} represents their covariance. The SSIM loss is implemented as $\mathcal{L}_{SSIM} = 1 - SSIM(I_{CBCT}, I_{Sim\text{-}CT})$, thereby minimizing structural dissimilarity between the two images. By giving this term, the largest weight ($\omega_{SSIM} = 1.0$), the model prioritizes anatomical fidelity during optimization.

The NCC Loss, $\mathcal{L}_{NCC}$, complements SSIM by focusing on global intensity alignment. It compensates for intensity variations arising from scatter, beam hardening, or reconstruction inconsistencies in CBCT. NCC is computed as the correlation coefficient between the mean-centered intensities of the two volumes [17]:

$$\mathcal{L}_{NCC} = -\frac{\sum_{x,y,z}(I_{CBCT}(x,y,z) - \mu_{CBCT})(I_{Sim-CT}(x,y,z) - \mu_{Sim-CT})}{\sqrt{\sum_{x,y,z}(I_{CBCT}(x,y,z) - \mu_{CBCT})^2 \sum_{x,y,z}(I_{Sim-CT}(x,y,z) - \mu_{Sim-CT})^2}} \quad (3)$$

where $I_{CBCT}(x, y, z)$ and $I_{Sim-CT}(x, y, z)$ represent the intensity values of the CBCT and sim-CT volumes at voxel (x, y, z), and μ_{CBCT}, μ_{Sim-CT} denote their respective global mean intensities.

To further ensure modality invariance, a MI term, $\mathcal{L}_{MI}$, was introduced. MI measures the shared statistical dependency between CBCT and Sim-CT intensity distributions, encouraging alignment even when the two modalities exhibit non-linear intensity mappings or contrast bias [8]. This loss is estimated using discretized joint intensity histograms with 32 bins per volume, and computed as the negative MI:

$$\mathcal{L}_{MI} = -[H(I_{CBCT}) + H(I_{Sim-CT}) - H(I_{CBCT}, I_{Sim-CT})] \quad (4)$$

where $H(\cdot)$ and $H(\cdot, \cdot)$ denote marginal and joint entropies, respectively. This formulation helps the model maintain robustness across varying acquisition conditions, noise levels, and contrast responses.

In addition, a gradient regularization term, $\mathcal{L}_{Grag}$, is included to encourage smoothness in the estimated sampling grid by penalizing large local spatial gradients, thereby reducing artifacts or unrealistic deformations.

Finally, a weak L2 regularization term, $\mathcal{L}_{reg}$, is applied to constrain the magnitude of rotation and translation parameters, ensuring physically plausible motion estimates, and avoiding overfitting. The weighting coefficients were empirically determined as $\omega_{SSIM} = 1.0$, $\omega_{NCC} = 0.1$, $\omega_{MI} = 0.1$, and $\omega_{Grad} = 0.1$.

2.4. Training Strategy

All models were implemented in PyTorch 1.11.3 with Python 3.10.12 and trained on a workstation equipped with an Intel Core i7-8700K CPU and an NVIDIA GeForce RTX 3090 GPU (24 GB VRAM). Mixed-precision computation was enabled through CUDA 11.3 and cuDNN to improve computational efficiency. The network was optimized using the Adam optimizer with an initial learning rate of 1×10^{-4}, by a factor of 0.5 every 100 epochs. Due to 3D memory constraints, a batch size of 1 was used, and training was conducted for 500 epochs. The composite loss function described in Section 2.3 was applied throughout training, balancing the

contributions of SSIM, NCC, and MI. This configuration stabilized gradient updates and improved registration accuracy across varying CBCT geometries and intensity conditions.

3. Results

The proposed 3D rigid-registration network was evaluated using paired CBCT and Sim-CT datasets generated with controlled translational and rotational displacements. Each dataset included predefined motion offsets that were applied before reconstruction, and the registration performance was assessed through both visual comparison and quantitative alignment accuracy.

As shown in Fig. 4(a–f), representative results for a translational motion case are presented. The CBCT (moving) image (a) shows a spatial shift relative to the reference Sim-CT (c). After applying the proposed network-based registration, the aligned image (b) became spatially consistent with the reference. The difference maps before and after registration (d–e) reveal a distinct reduction in residual intensity along the phantom boundary and internal structures. The RGB overlay (f) confirms that the contours of the registered CBCT and Sim-CT volumes were well aligned.

In contrast, 5(a–f), a representative rotational motion case demonstrates similar registration performance. Prior to registration, the CBCT and Sim-CT volumes exhibited a noticeable angular deviation, which was corrected after processing by the proposed network. The post-registration image (b) demonstrated close correspondence with the reference (c), and the difference map (e) showed a clear reduction in residual error compared with the initial state (d). The overlay view (f) indicates that the circular boundary of the phantom was accurately realigned with minimal visible discrepancy. Fig. 4(a–f) and 5(a–f) show representative results for translational and rotational motion cases, respectively. These results demonstrate that the proposed network effectively aligns CBCT volumes with reference Sim-CT images under various motion displacements.

The convergence characteristics of the predicted rigid motion parameters during training for the 1.5 cm translation case are illustrated in Fig. 6(a–b). The translational

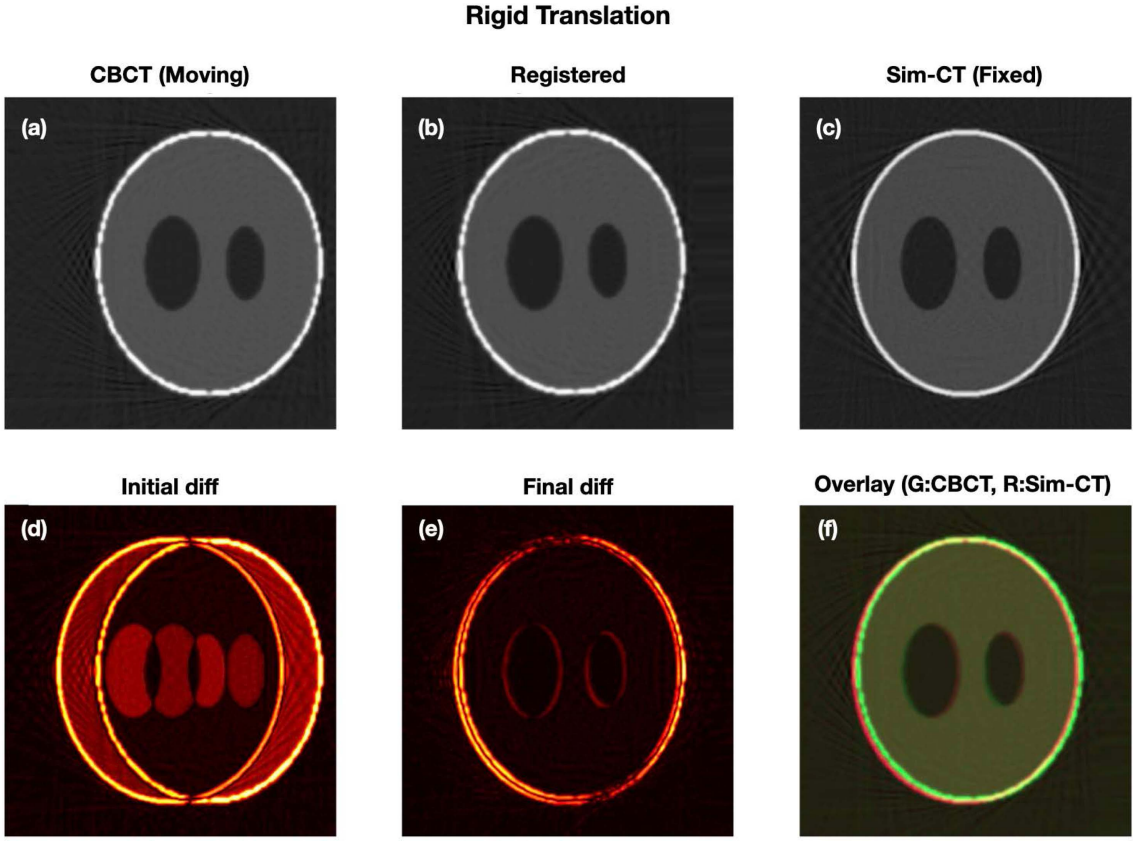

Fig. 4. (Color online) Representative slice showing rigid translation correction between the moving CBCT and fixed Sim-CT volumes. (a) CBCT (moving), (b) registered output, and (c) Sim-CT (fixed) images. (d) Initial difference before registration, (e) final difference after registration, and (f) RGB overlay of CBCT (green) and registered Sim-CT (red).

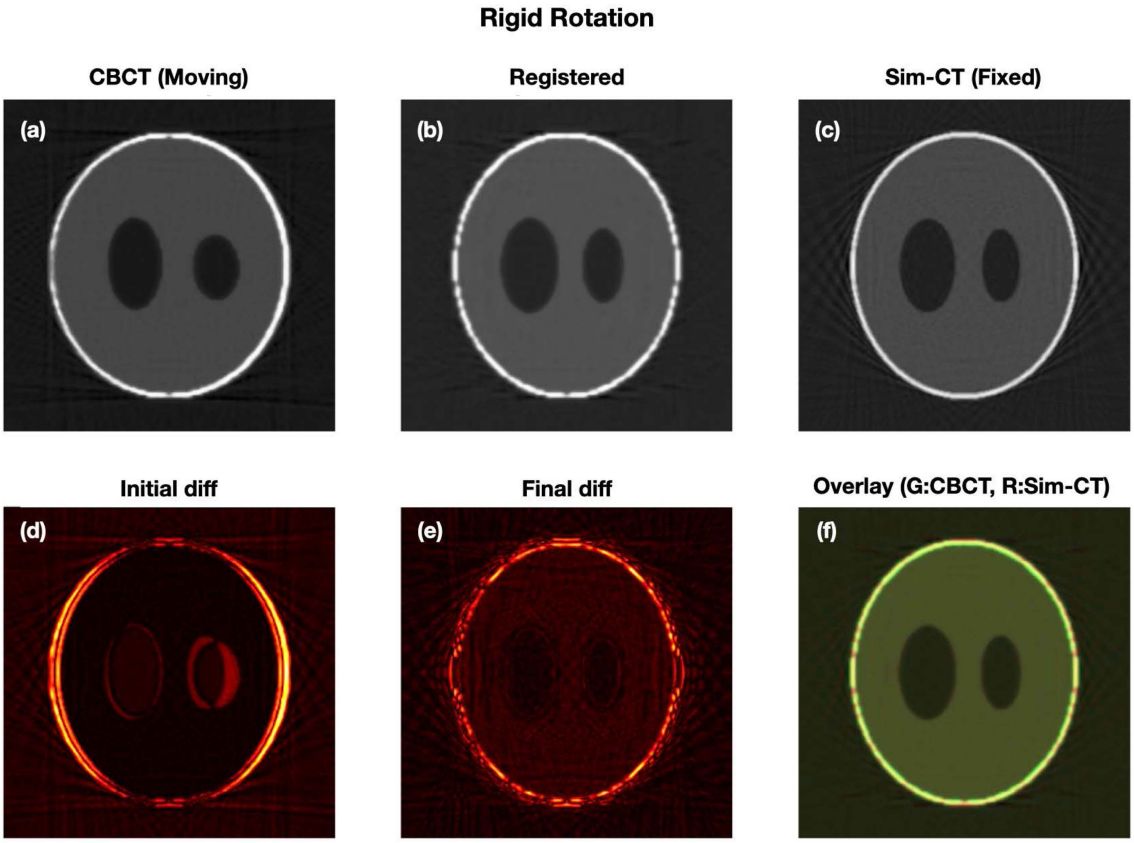

Fig. 5. (Color online) Results of rigid rotational correction between the CBCT and Sim-CT volumes. (a) CBCT (moving), (b) registered output, and (c) Sim-CT (fixed) images. (d) Initial difference before registration, (e) final difference after registration, and (f) RGB overlay of CBCT (green) and registered Sim-CT (red).

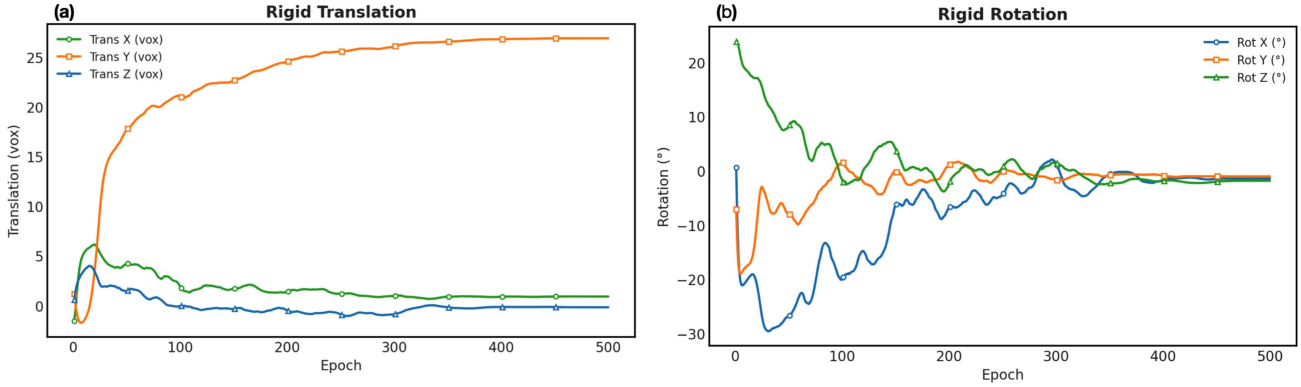

Fig. 6. (Color online) Convergence behavior of the predicted rigid motion parameters during network training for the 1.5 cm translation case. (a) Translational displacements along the X, Y, and Z axes are shown in voxel units, and (b) rotational displacements around each axis (θ_x, θ_y, θ_z) are presented in degrees. All parameters gradually stabilized after approximately 300 epochs, indicating convergence of the optimization process toward consistent motion estimation.

parameters in Fig. 6(a)—along the X, Y, and Z axes—exhibited smooth convergence toward stable displacement values, while the rotational parameters in Fig. 6(b)—around each axis (θ_x, θ_y, θ_z) —demonstrated similar stabilization after approximately 300 epochs. This behavior indicates that the optimization process successfully reached a steady state without oscillation, ensuring consistent estimation of both translational and rotational components throughout the training iterations.

Quantitative evaluation of the estimated rigid para-

Table 1. Mean absolute translational errors (mean ± SD) between estimated and ground-truth rigid parameters under different motion conditions.

Motion condition	Translations (mm)		
	[Δtx]	[Δty]	[Δtz]
Translation (1.5 cm)	1.28 ± 0.16	0.98 ± 0.09	1.39 ± 0.20
All cases	1.31 ± 0.17	1.05 ± 0.13	1.58 ± 0.28

Table 2. Mean absolute rotational errors (mean ± SD) between estimated and ground-truth rigid parameters under different motion conditions.

Motion condition	Rotations (°)		
	[$\Delta\theta_x$]	[$\Delta\theta_y$]	[$\Delta\theta_z$]
Rotation ($\theta_x = 30°$)	0.32 ± 0.11	0.21 ± 0.08	0.55 ± 0.14
All cases	0.43 ± 0.15	0.33 ± 0.13	0.71 ± 0.18

meters is summarized in Tables 1 and 2. For translational displacements, the mean absolute errors were 1.28 ± 0.16 mm, 0.98 ± 0.09 mm, and 1.39 ± 0.20 mm along the x, y, and z axes, respectively. Across all motion conditions, the average translational errors remained within approximately 2 mm, indicating accurate recovery of the spatial offsets. The corresponding rotational errors were 0.32 ± 0.11°, 0.21 ± 0.08°, and 0.55 ± 0.14° for the x, y, and z axes, respectively, and all cases showed angular deviations below 1°. These results confirm the quantitative consistency of the proposed network in estimating six-degree-of-freedom rigid motion parameters under both translational and rotational perturbations.

4. Dicussion and Conclusions

Conventional intensity-based registration algorithms (e.g., NCC, MI) primarily rely on voxel-wise intensity similarity and represent anatomical structures only indirectly through gradient information. As a result, these methods may be prone to local minima and unstable convergence, particularly when significant appearance differences exist between modalities or when intensity distributions between CBCT and Sim-CT are inconsistent due to scatter, beam hardening, or nonlinear reconstruction artifacts [18, 19]. Previous studies have also indicated that conventional intensity-based registration algorithms are often prone to local minima and depend strongly on initialization, which can limit their optimization efficiency and make convergence less effective in complex search spaces [20].

To address these limitations, a three-dimensional deep-learning–based rigid-registration framework was developed to estimate full 6-DoF motion between CBCT and Sim-CT volumes. The proposed network consistently recovered both translations and rotations, effectively compensating for inter-scan misalignment. Quantitatively, mean absolute translational errors were below 2 mm, and rotational errors were within 1°. In the representative 1.5 cm translation case, displacements across all axes remained $\leq$ 1.5 mm, and the 30° rotation case exhibited angular errors of approximately 1°. The convergence profiles in Fig. 6(a–b) indicate that all motion parameters stabilized after approximately 300 epochs without oscillation, demonstrating consistent optimization behavior.

The proposed model performs single feed-forward inference using a pre-trained network, enabling near real-time estimation of 6-DoF motion parameters. By leveraging SSIM-based structural similarity as the primary loss and auxiliary intensity metrics (NCC, MI), the model maintained robustness against CBCT-specific nonlinearities and truncation artifacts. This single-pass inference framework demonstrated stable and low-variance alignment performance across all motion conditions, indicating that real-time rigid registration may be achievable through a single feed-forward inference process. The proposed network effectively maintained robustness against CBCT-specific nonlinearities and truncation artifacts, achieving sub-millimeter/sub-degree accuracy across diverse motion scenarios [18].

Precise CBCT–CT alignment remains essential for adaptive radiotherapy (ART), as residual misregistration can lead to inaccuracies in dose accumulation and compromise anatomical consistency [21]. Because the proposed framework operates directly on reconstructed 3D volumes without requiring access to raw projection data, it can be seamlessly integrated into existing on-board imaging workflows for daily setup verification or adaptive CBCT registration. Although explicit runtime benchmarking was not performed, the lightweight architecture and single-pass inference design suggest strong feasibility for near real-time clinical deployment using GPU acceleration. These findings indicate that the proposed deep-learning–based rigid-registration framework can serve as a robust and scalable component for motion correction and geometry-consistent adaptive image guidance in modern IGRT/ART systems.

This study has certain limitations. Validation was conducted using numerically simulated phantoms under controlled motion, which may not fully represent patient-specific variability or CBCT artifacts such as scatter and beam hardening. Furthermore, the current implementation assumes rigid-body motion; extending this framework to hybrid CNN–Transformer architectures for deformable

registration is a natural next step. Furthermore, deep learning–based denoising and image enhancement methods have demonstrated substantial improvements in CT and CBCT image quality by suppressing noise and preserving structural details, which could complement the proposed registration framework in clinical adaptive workflows [22]. Additional evaluation using perceptual metrics such as SSIM or NGF could provide deeper insight into local alignment fidelity. Finally, validation with clinical datasets and prospective runtime evaluation will be required to substantiate its applicability to on-line adaptive radiotherapy workflows, where real-time image registration and dose adaptation must be achieved within the treatment session.

In summary, the proposed 3D deep-learning–based rigid-registration framework demonstrated sub-millimeter and sub-degree precision in estimating 6-DoF motion between CBCT and Sim-CT volumes, with stable convergence and high computational efficiency. These findings support its potential as a robust, scalable component for motion correction and geometry-consistent image guidance in modern IGRT/ART systems.

Acknowledgment

This work was supported by Dongseo University 『Dongseo Frontier Project』 Research Fund of 2025.

References

[1] X. Jia, H. Yan, X. Gu, and S. B. Jiang, Phys. Med. Biol. **57**, 577 (2012).
[2] B. Jo, K. Park, D. Shin, Y. K. Lim, J. H. Jeong, S. B. Lee, H.-J. Kim, and H. Kim, Appl. Sci. **11**, 2592 (2021).
[3] K. Srinivasan, M. Mohammadi, and J. Shepherd, Pol. J. Radiol. **79**, 181 (2014).
[4] G. Jarry, S. A. Graham, D. J. Moseley, D. J. Jaffray, J. H. Siewerdsen, and F. Verhaegen, Med. Phys. **33**, 4320 (2006).
[5] L. Zhu, Y. Xie, J. Wang, and L. Xing, Med. Phys. **36**, 2258 (2009).
[6] X. Zhen, X. Gu, H. Yan, L. Zhou, X. Jia, and S. B. Jiang, Phys. Med. Biol. **57**, 6807 (2012).
[7] C. K. Glide-Hurst, P. Lee, A. D. Yock, J. R. Olsen, M. Cao, F. Siddiqui, W. Parker, A. Doemer, Y. Rong, A. U. Kishan, S. H. Benedict, X. A. Li, B. A. Erickson, J. W. Sohn, Y. Xiao, and E. Wuthrick, Int. J. Radiat. Oncol. Biol. Phys. **109**, 1054 (2021).
[8] P. A. Legg, P. L. Rosin, D. Marshall, and J. E. Morgan, Comput. Med. Imaging Graph. **37**, 597 (2013).
[9] B. Jo, J. Magn. **28**, 403 (2023).
[10] A. Sisniega, W. Zbijewski, A. Badal, I. S. Kyprianou, J. W. Stayman, J. J. Vaquero, and J. H. Siewerdsen, Med. Phys. **40**, 051915 (2013).
[11] H. Liu, D. Schaal, H. Curry, R. Clark, A. Magliari, P. Kupelian, D. Khuntia, and S. Beriwal, Radiat. Oncol. **18**, 144 (2023).
[12] Y. Fu, Y. Lei, T. Wang, W. J. Curran, T. Liu, and X. Yang, Phys. Med. Biol. **65**, 20TR01 (2020).
[13] G. Balakrishnan, A. Zhao, M. R. Sabuncu, J. Guttag, and A. V. Dalca, IEEE Trans. Med. Imaging **38**, 1788 (2019).
[14] J. Chen, E. C. Frey, Y. He, W. P. Segars, Y. Li, and Y. Du, Med. Image Anal. **82**, 102615 (2022).
[15] A. Biguri, M. Dosanjh, S. Hancock, and M. Soleimani, Biomed. Phys. Eng. Express **2**, 055010 (2016).
[16] Z. Wang, A. C. Bovik, H. R. Sheikh, and E. P. Simoncelli, IEEE Trans. Image Process. **13**, 600 (2004).
[17] D. M. Tsai, C. T. Lin, and J. F. Chen, Pattern. Recognit. Lett. **24**, 2525 (2003).
[18] H. Park, W. Plishker, H. Quon, J. Wong, R. Shekhar, J. Lee, Phys. Med. Biol. **62**, 927 (2017).
[19] M. Abdel-Basset, A. E. Fakhry, I. El-Henawy, T. Qiu, A. K. Sangaiah, J. Med. Syst. **41**, 197 (2017).
[20] G. Song, J. Han, Y. Zhao, Z. Wang, H. Du, Curr. Med. Imaging **13**, 274 (2017).
[21] H. Ghaznavi, B. Maraghechi, H. Zhang, T. Zhu, E. Laugeman, T. Zhang, T. Zhao, T. R. Mazur, and A. Darafsheh, Phys. Med. Biol. **70**, 09TR01 (2025).
[22] C.-Y. Park and B.-D. Jo, J. Magn. **29**, 550 (2024).